Journal of Computational Applied Mechanics 2025, 56(4): 802-824

DOI: 10.22059/jcamech.2025.398462.1545

RESEARCH PAPER

Influence of Hall Current and Entropy Generation Effects on Squeezing Flow with Homogeneous and Heterogeneous Chemical Reactions

Naseer Khan [a], Muhammad Farooq [a], Wajid Ullah Jan [a], Ibrahim Alraddadi [b, *], Mohamed Omri [c], Lotfi Ladhar [d], Hijaz Ahmad [b, e, f]

[a] *Department of Mathematics, Abdul Wali Khan University Mardan (23200), KP, Pakistan*
[b] *Department of Mathematics, Faculty of Science, Islamic University of Madinah, Madinah, Saudi Arabia*
[c] *Deanship of Scientific Research, King Abdulaziz University, Jeddah, Saudi Arabia*
[d] *Department of Electrical and Computer Engineering, Faculty of Engineering, King Abdul Aziz University, Jeddah21589, Saudi Arabia*
[e] *Operational Research Center in Healthcare, Near East University, Nicosia/TRNC, 99138 Mersin 10, Turkey*
[f] *Department of Mathematics, College of Science, Korea University, 145 Anam-ro, Seongbuk-gu, Seoul 02841, South Korea*

Abstract

This study investigates the combined effects of the Hall current and entropy generation, taking into account Joule heating and viscous dissipation, on the squeezing flow of a viscous fluid between two parallel plates in the presence of both homogeneous and heterogeneous chemical reactions. The primary objective is to enhance understanding of heat transfer rates relevant to applications such as fuel cells, engine cooling systems, pharmaceutical processes, and various engineering industries. In the problem under consideration, the upper plate is squeezing down to the bottom plate, whereas the lower plate exhibits the irreversibly analysis of flow with homogeneous and heterogeneous chemical reactions. When the problem is modeled, the coupled system of partial differential equations is obtained which is transformed into a system of ordinary differential equations by applying the similarity transformation. These resulting equations are solved using the Homotopy Analysis Method (HAM), with appropriate initial conditions and auxiliary parameters to ensure rapid and reliable convergence. The accuracy of the HAM solutions is validated by comparison with results obtained using the numerical solver BVP4c. The study further analyzes effects of the Hall term, entropy generation, variable viscosity, and thermal conductivity on the velocity and temperature distributions in the presence of chemical reactions.

Keywords: Squeezing Flow; Entropy Generation; Homogeneous–Heterogeneous Reactions; Homotopy Analysis Method; Variable Viscosity and Thermal Conductivity; BVP4c Method, Hall Effects; viscous Fluid.

1. Introduction

One of the most significant types of flow is the flow of a viscous substance, which is squeezing among parallel plates. Squeezing flow is significant in a variety of sectors, including injection, liquid-metal molding, water heating,

* Corresponding author: ialraddadi@iu.edu.sa

cooling, squeezed films in power transmission, lubricated bearings, and compression. Nanoliquids are colloidal suspensions of solid particles in traditionally used working materials that range in size from 1 to 100 nm. The most often utilized forms of metals include metallic oxides (TiO2, Al2O3, CuO), carbon nanotubes, nitride (SiN, SiC, TiC), and nanoparticles (Cu, Ag, Au, Fe). Enclosing nanoparticles within traditionally used materials improves their ability to conduct heat. Nanoparticles find extensive use in computer processors, air conditioners, compressors, combustors, heat exchangers, and hybrid powered engines, among other devices. Because of its many practical applications for examining the heat transmission and velocity field between the squeezing plates, researchers are very interested in this area. [1] Carried out the preliminary work on the squeezing flow and conducted study on the lubricating system. The scientist's area of study on squeezing flow was expanded by Stefan. In the recent years a number of scholars have been advanced to the investigation of the squeezing flow. Using the procedure of homotopy analysis method (HAM), Analytical results was obtained by [2] for the quasi steady axi-symmetric newtonian fluid, which is squeezing among two parallel plates. A turbulent, squeezing flow involving heat and mass transfer among squeezing plates was examined by [3], [4] used a neural network to study the nanofluid of a constricted conduit.

He looked at the impact of the Reynolds number, power law index, growth ratio, and nanopartical absorption on this problem. [5] investigated how convective circumstances and chemical reactions affect squeezing flow, coverlet flow has received the majority of attention. [6] Has lately looked at the effects of solvent, heat, and velocity on the transportation characteristics of the squeezed fluid. When the Darcy parameter increases, the profile of fluid velocity close to both plate's decreases and the flow encounters greater resistance. In a theoretical analysis, [7] shown how the gripping flow of water establish on carbon nano-tubes could be affected by thermal radiation on a Darcy Forch-heimer permeable size of medium. [8] Has suggested in a different study to theoretically examine the interaction between the Sutter by fluid's fluency in the squeezed tube, also they effect thermal radiation and chemical reactions. Cortell conducted a study on it lately [9]. The main purpose for the reduction in thermal boundary sheet thickness is nonlinear thermal radiation, which also increases the Prandtl number P_r, and affects how heat is transmitted across an expanded sheet. [10] Has recently investigated Jeffrey nanofluid's nonlinear thermal effects on three-dimensional flow. The increment functions of temperature parametric radiation and absorption of nanoparticles were also attained. In his research [11] investigated the flow of a nano-fluid of a second-grade on a boundary sheet that was three-dimensional, as well as its transformation into a nanoparticle-operating fluid and the response of solar radiations to it.

The effect of a uniform transverse magnetic field on the flow of an incompressible, viscous electrically conducting fluid between two infinitely parallel, motionless, and insulating plates was investigated by [12]. It was possible to expand the challenge in several ways. A variety of physical effects were used to derive closed-form solutions for the velocity fields [13, 14]. You may find numerical and precise solutions to the heat transport issue in references [15, 16]. Since the Hall term has little and moderate impact on tiny and moderate magnetic field values, it was disregarded while using Ohm's law in the aforementioned circumstances. But nowadays magneto hydrodynamics is used more and more in situations where a high magnetic field is present, where the effect of electromagnetic force is more apparent [17]. In these cases, the Hall current is crucial because it significantly affects the direction and amplitude of the current density, and hence the magnetic force. A steady-state flow of electrically conducting and viscous fluids via tubes was investigated by [18] in relation to the Hall effect. Hall currents were investigated by [19, 20] in relation to the steady-state MHD Couette flow including heat transfer. It was thought that the two plates' temperatures would either remain constant or change linearly with the flow direction. Hall currents were investigated by [21] in relation to a uniformly suctioned and injected constant Hartmann flow at the boundary plates. Expanding the problem to the unsteady state with heat transfer was done by [22].

Accordingly, this research aims to examine the consequences of homogeneous and heterogeneous chemical reactions on squeezing flows between parallel plates under the influence of Hall current and viscous dissipation.

Using similarity transformations, the proposed model has been converted into a non-similar coupled partial differential equation. The governing equations have been solved numerically through the application of Homotopy analysis and BVP4C techniques. Finally, the results of this study have been graphically discussed for a variety of configurations of the parameters that are already known.

2. Mathematical Formulation of the Problem

Here we take a laminar, axi-symmetric, incompressible, and viscous fluid flow in the middle of two parallel, horizontally squeezing plates considering with the Hall current in Fig 1. We separate the two plates from each other by a distance of $h(t) = \sqrt{1-\alpha t}$ Here, the length of separation is l, which shows the separation of plates at $t = 0$, as shown in figure (1). Squeezing both plates till $\alpha > 0$ until they touch each other at $t = 1/\alpha$, both

plates are separated for $\alpha < 0$. A uniform magnetic field, $B^*(t) = \frac{B_0^*}{\sqrt{1-\alpha t}}$ is also applied in the y - direction on the velocity profile. The constant temperatures of both upper and lower plates are assumed to be ξ_i and ξ_j respectively. Heat transfer is studied in the context of thermal radiation. The model was analyzed by [23] for both homogeneous and heterogeneous chemical reactions.
The homogeneous cubic autocatalysis reaction takes the following form:

$$\Omega_1 + 2\Omega_2 \Rightarrow 3\Omega_2 \tag{1}$$

And the concentration rate is $K_c a^* (b^*)^2$ whereas heterogeneous reaction on the catalyst surface, is expressed by

$$\Omega_1 \Rightarrow \Omega_2, \tag{2}$$

a^* and b^*, respectively, represent the concentration of the chemical species Ω_1 and Ω_2 while $k_c{}^*$ represents the rate constants. As seen by the following equations, the reaction rate in external flow disappears behind the boundary layer edge.

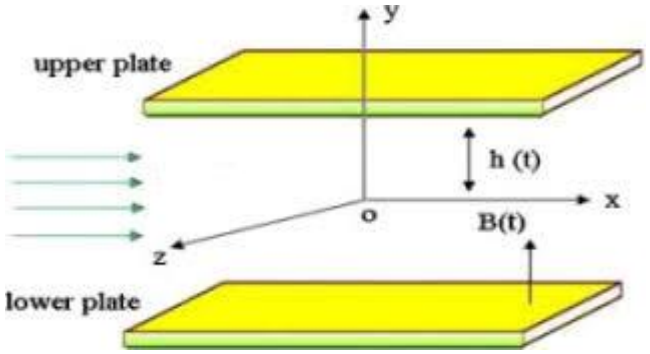

Fig 1: Problem Geometry

In the Cartesian coordinate system (x, y), we derive the equations governing the conservation of mass, momentum, and thermal energy, as well as those pertaining to homogeneous and heterogeneous chemical processes [24-27].
Mass conservation equation is expressed as,

$$\frac{\partial \Psi}{\partial x} + \frac{\partial v}{\partial y} = 0, \tag{3}$$

Conservation equation of momentum is expressed as,

$$\frac{\partial \Psi}{\partial t} + \Psi \frac{\partial \Psi}{\partial x} + v \frac{\partial \Psi}{\partial y} = -\frac{1}{\rho}\frac{\partial p}{\partial x} + \frac{\mu}{\rho}\left[\frac{\partial^2 \Psi}{\partial x^2} + \frac{\partial^2 \Psi}{\partial y^2}\right] - \frac{\sigma {B_0}^2}{1+m^2}(\Psi - mv), \tag{4}$$

$$\frac{\partial v}{\partial t} + \Psi \frac{\partial v}{\partial x} + v \frac{\partial v}{\partial y} = -\frac{1}{\rho}\frac{\partial p}{\partial y} + \frac{\mu}{\rho}\left[\frac{\partial^2 v}{\partial x^2} + \frac{\partial^2 v}{\partial y^2}\right] - \frac{\sigma {B_0}^2}{1+m^2}(\Psi + mv), \tag{5}$$

Energy equation for Joule heating and viscous dissipation is as follows:

$$\frac{\partial \xi}{\partial t}+\Psi\frac{\partial \xi}{\partial x}+\nu\frac{\partial \xi}{\partial y}=-\frac{\kappa^{*}}{\rho C_{p}}\left[\frac{\partial^{2}\xi}{\partial x^{2}}+\frac{\partial^{2}\xi}{\partial y^{2}}\right]+(\Psi^{2}+\nu^{2})+\frac{2\mu}{\rho C_{p}}\left[\left(\frac{\partial \Psi}{\partial x}\right)^{2}+\left(\frac{\partial \Psi}{\partial y}\right)^{2}+\left(\frac{\partial \Psi}{\partial x}+\frac{\partial \Psi}{\partial y}\right)^{2}\right]$$
$$-\frac{2}{3}\left(\frac{\partial \Psi}{\partial x}+\frac{\partial \nu}{\partial y}\right)^{2}-\frac{\sigma {B_{0}}^{2}}{1+m^{2}}(\Psi), \tag{6}$$

Similarly equations for homogeneous and heterogeneous reactions are given by,

$$\frac{\partial a^{*}}{\partial t}+\Psi\frac{\partial a^{*}}{\partial x}+\nu\frac{\partial a^{*}}{\partial y}=D_{\Omega}\frac{\partial^{2}a^{*}}{\partial y^{2}}-{K_{c}}^{*}a^{*}(b^{*})^{2}, \tag{7}$$

$$\frac{\partial b^{*}}{\partial t}+\Psi\frac{\partial b^{*}}{\partial x}+\nu\frac{\partial b^{*}}{\partial y}=D_{B}\frac{\partial^{2}b^{*}}{\partial y^{2}}+{K_{c}}^{*}a^{*}(b^{*})^{2}. \tag{8}$$

For following equations we used Ψ,ν which represents the recursive elements of the horizontal and vertical velocity, where p is the pressure of fluid and $\boldsymbol{\xi}$ is the temperature distribution, the homogeneous and heterogeneous response variables are $a*$ and $b*$. The fluid density is expressed in terms of ρ. The fluid heat capacity is C_{p}, and its electrical conductivity is σ. The chemical species associated with $B*$ and $\boldsymbol{\Omega}$ diffusion coefficients are displayed by the variables $D_{\boldsymbol{\Omega}}$ and $D_{B}*$,respectively. Thermal conductivity is expressed by $\boldsymbol{\kappa}$ and permeability by K*. Assuming that the Hall parameter, denoted by m, is $m=\sigma\beta B_{0}$.

3. Similarity Transformation Approach For Boundary Conditions

The following criteria were established for the problem's boundaries:

$$\Psi=0,\nu=0,\xi=\xi_{l},D_{\Omega}\frac{\partial a^{*}}{\partial y}=\Gamma_{2}a^{*},{D_{B}}^{*}\frac{\partial b^{*}}{\partial y}=-\Gamma_{2}a^{*}, \quad \text{at} \quad y=0. \tag{9}$$

$$\Psi=0,\nu=\frac{\alpha D}{2\sqrt{1-\alpha t}},\xi=\xi_{\psi},a^{*}={a_{0}}^{*},b^{*}=0. \quad \text{at} \quad y=h\,(t). \tag{10}$$

By applying the following similarity transformations approach, an ordinary differential equation system was derived from a system of partial differential equations [28].

$$\Psi=\frac{\alpha x\Phi'(\Upsilon)}{2(1-\alpha t)},\nu=\frac{-\alpha l\Phi(\Upsilon)}{2\sqrt{1-\alpha t}},\xi=\vartheta(\Upsilon)\xi_{j},\Upsilon=\frac{y}{l\sqrt{1-\alpha t}}. \tag{11}$$

And

$$a={a_{0}}^{*}\boldsymbol{\Phi}(\boldsymbol{\Upsilon}),b^{*}={a_{0}}^{*}\text{Ģ}(\boldsymbol{\Upsilon}),B^{*}(t)=\frac{{B_{0}}^{*}}{\sqrt{1-\boldsymbol{\alpha t}}_{j}},\boldsymbol{\vartheta}=\frac{\boldsymbol{\xi}-\boldsymbol{\xi}_{i}}{\boldsymbol{\xi}-\boldsymbol{\xi}_{i}}. \tag{12}$$

The form of the homogeneous, heterogeneous, momentum, and energy equations as follows, where the continuity equation (3) is identically satisfied.

$$\Phi''''-S_r\left(\Phi''\Phi'+2\Phi''-\Phi\Phi'''+\Upsilon\Phi'''\right)-\varphi(a^*)^2L\left(\frac{1}{1+m^2}\Phi''+\frac{m}{1+m^2}R_e\Phi'\right)=0. \tag{13}$$

$$\vartheta''-P_rS_r\left(\Upsilon\vartheta'-\Phi\vartheta'-2NE_2\Phi'^2-N\delta E_1\Phi''^2-\frac{M}{1+m^2}(G_1\Phi'^2+G_2\Phi^2)\right)=0. \tag{14}$$

$$\varphi''-2S_rS_c^*\left(\Upsilon\varphi'-\Phi\varphi'+\Gamma_1\varphi\Ģ^2\right)=0. \tag{15}$$

$$\Ģ''\beta-S_rS_c^*\left(\Upsilon\Ģ'-\Phi\Ģ'-\Gamma_1\varphi\Ģ^2\right)=0\,. \tag{16}$$

On the same way, the transformation of the boundary conditions change to

$$\Phi(0)=0,\Phi'(0)=0,\vartheta(0)=1,\varphi'(0)=\Gamma_2\varphi(0),\beta\Ģ'(0)=-\Gamma_2\varphi(0), \tag{17}$$

$$\Phi(1)=0.5,\Phi'(1)=0,\vartheta(1)=0,\varphi(1)=1,\Ģ(1)=0. \tag{18}$$

In this problem, the squeezed Reynolds number is $S_r=\alpha l^2/2\nu$, $\varphi a^*=lB_0\sqrt{\frac{\sigma}{\mu}}$, is the Hartman number, $P_r=\mu C_p/\kappa$,is the Prandtl parameter, $S^*{}_c=\nu/D_\Omega$ is the Schmidt parameter, the homogeneous reaction strength is $\Gamma_1=(2K_c\left(a_0*\right)^2(1-\alpha t))/\alpha$, and the heterogeneous reaction strength is $\Gamma_2=K_c/D_\Omega$, Reynolds number is $R_e=\frac{1}{x}\sqrt{\frac{\eta_1(1-\alpha t)}{\mu}}$, the Grashof number is $G_1=\frac{\alpha x^2}{2b\xi_l(1-\alpha t)^2}\sqrt{\frac{\eta_1}{\mu}}$,whereas $G_2=\frac{\alpha\eta_1}{2\mu\xi_l(1-\alpha t)}$ the Brinkman number, $\alpha=\frac{l}{b}\sqrt{\frac{\eta_1}{\mu}}$, is the couple stress parameter. The effects of couple-stress are significant for large values of $\alpha=\frac{l}{b}$, where $l=\sqrt{\frac{\eta_1}{\mu}}$, is the material constant. $L=\rho(1-\alpha t)/B_0$ is the convection or buoyancy parameter, $E_1=\frac{\alpha^2x^2}{\xi_l(1-\alpha t)^2}$ is the local Eckret number, $E_2=\frac{\alpha^2}{\xi_l(1-\alpha t)}$ is the Eckert number, $M=\sigma\left(B_0\right)^2$ is the magnetic parameter, $N=\nu/\rho C_p$ is a porosity number, $\delta=1/l^2$ is a small parameter, $\beta=D_\Omega/D_B*$ is represent the diffusion coefficient ratio. Here, we assume that Ω and B* is the coefficients of diffusion for chemical species of identical sizes. The alternative theory states that D_Ω and D_B*are comparable, hence $\beta = D_\Omega/D_B*=1$, also $\Ģ(\Upsilon)+\varphi(\Upsilon)=1$. [29]

3.1 Important Constants

In engineering, the Sherwood number ($S_rh.$), the coefficient of skin friction (C_Φ), and the local Nusselt parameter ($N\psi$) are a few of the coefficients of importance. Which are define as below,

$$C_\Phi{}^*=\left(S_r/h\right)=\Phi''(0),-\vartheta'(0)=N\psi,\ -\Ģ'(0)=-\varphi'(0)=S_rh.$$

4. Analysis of control convergence parameters

It is significant to notice that the non-zero auxiliary parameters $\hbar_{\Phi}$, ,$\hbar_{\vartheta}$, $\hbar_{\varphi}$, and $\hbar_{Ç}$ in the series solutions, where the homotopy series solutions converge and how quickly they do it. The "Method of average residual error" present by [19]was applied to determine the ideal values for $\hbar_{\Phi}$, ,$\hbar_{\vartheta}$, $\hbar_{\varphi}$, and $\hbar_{Ç}$.

$$\varepsilon_{\psi}^{\Phi} = \frac{1}{\ell+1}\sum_{j=0}^{\ell}\left[N\Phi\left(\sum_{i=0}^{\psi}\tilde{\Phi}(\emptyset),\sum_{i=0}^{\psi}\tilde{\vartheta}(\emptyset)\right)\right]^2 d\emptyset, \tag{19}$$

$$\varepsilon_{\psi}^{\vartheta} = \frac{1}{\ell+1}\sum_{j=0}^{\ell}\left[N\vartheta\left(\sum_{i=0}^{\psi}\tilde{\Phi}(\emptyset),\sum_{i=0}^{\psi}\tilde{\vartheta}(\emptyset)\right)_{n=jD_u n}\right]^2 d\emptyset, \tag{20}$$

$$\varepsilon_{\psi}^{\varphi} = \frac{1}{\ell+1}\sum_{j=0}^{\ell}\left[N\varphi\left(\sum_{i=0}^{\psi}\tilde{\Phi}(\emptyset),\sum_{i=0}^{\psi}\tilde{\varphi}(\emptyset),\sum_{i=0}^{\psi}\tilde{Ç}(\emptyset)\right)_{n=jD_u n}\right]^2 d\emptyset, \tag{21}$$

$$\varepsilon_{\psi}^{Ç} = \frac{1}{\ell+1}\sum_{j=0}^{\ell}\left[NÇ\left(\sum_{i=0}^{\psi}\tilde{\Phi}(\emptyset),\sum_{i=0}^{\psi}\tilde{\varphi}(\emptyset),\sum_{i=0}^{\psi}\tilde{Ç}(\emptyset)\right)_{n=jD_u n}\right]^2 d\emptyset, \tag{22}$$

In light of [30]

$$\varepsilon_{\psi}^{t} = \varepsilon_{\psi}^{\Phi} + \varepsilon_{\psi}^{\vartheta} + \varepsilon_{\psi}^{\varphi} + \varepsilon_{\psi}^{Ç} \tag{23}$$

ε_{ψ}^{t} is the representation of the entire squared residual error in this case. The overall method of average residual error is decreased using the Mathematica software ({BVPh 2.0}, 2014).

5. Discussion on Error Analysis

To make sure the analysis is reliable for lowest residual errors, an error analysis is performed. (HAM) and (BVP4C), respectively provide analytical and numerical solutions for the problem. 40th order of approximation is used for analysis. Additionally, utilizing the Mathematica package BVPh 2.0 for minimum residual error up to 10^{-40}, this study is assumed to be advance the dependability of (HAM) approaches.

Matlab is used to match the outcomes with the numerical solutions of (BVP4C), in order to verify the authenticity and accuracy of the HAM solution. The accuracy of both approaches for the many physical characteristics involved was examined using the error analysis, displayed in Figures (2) and Tables (1–17). The residual error for $\Phi(\Upsilon), \vartheta(\Upsilon), \varphi(\Upsilon)$ and $Ç(\Upsilon)$ is shown at different approximation orders in Figure 2. Continuous reduction of the error is observed up to the 20th order of approximation, as the sub-figures make evident, for each of the following specified values; G_1=0.1, G_2=0.1, R_e=0.2, m=0.1, L=0.2, δ=0.1, β=0.5, S^*_c=0.1, Γ_1=0.1, P_r=0.3, S_r=0.1, Γ_2=0.2, N=0.3, E_1=0.1, E_2=0.2, M=0.1 and φ a*=0.3. Cumulative residual error for each approximation order has been shown in Table 1 for specified values. Table 2 displays distinct average squared residual errors at different approximation orders for $\Phi''(\Upsilon)$, $-\vartheta'(\Upsilon)$, $-\varphi'(\Upsilon)$, *and* $Ç'(\Upsilon)$, with fixed values of $G_1 = 0.1$, $G_2 = 0.1$, $R_e = 0.2$, $m = 0.1$, $L = 0.2, \delta = 0.1, \beta = 0.5$, $S^*_c = 0.5, \Gamma_1 = 0.1$, $P_r = 0.5$, $S_r = 0.3, \Gamma_2 = 0.5$ and $N = 0.3$, $E_1 = 0.1$, $E_2 = 0.2$, $M = 0.3, \varphi a^* = 0.2$. The numerical and analytical values produced by HAM and BVP4c for a variety of Υ values are constructed with fixed values of other parameters in Table 3, such as G_1=0.1, G_2=0.1, R_e =0.2, m=0.1, L=0.2, δ=0.1, β=0.5, S^*_c=0.5, Γ_1=0.1, P_r=0.5, S_r=0.3, Γ_2=0.5 and N=0.3, E_1=0.1, E_2=0.2, M=0.3, φ a*=0.2. It demonstrates how well they great agreement with one another.

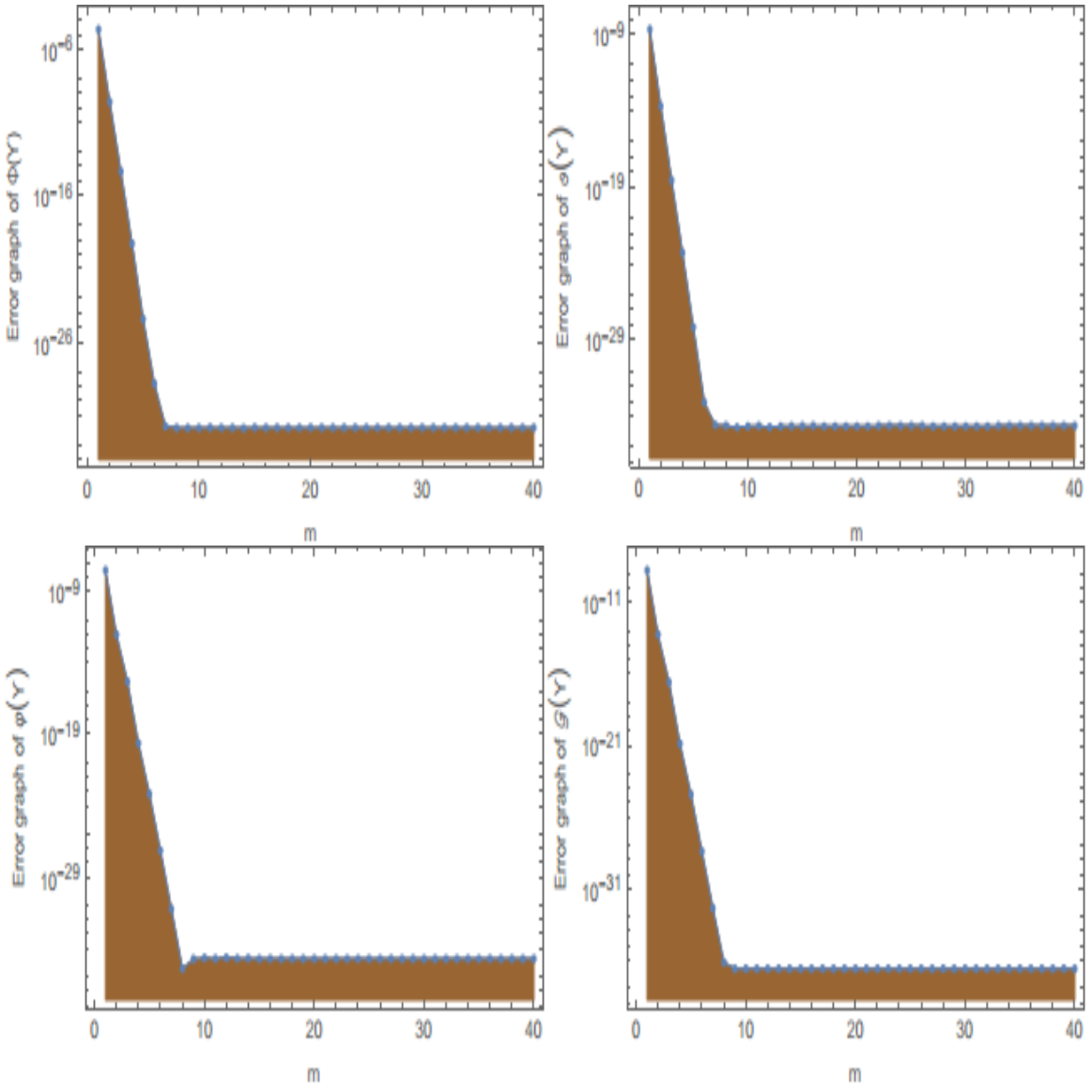

Figure 2: Individual error profiles of $\Phi(\Upsilon), \vartheta(\Upsilon), \varphi(\Upsilon)$ and $\zeta(\Upsilon)$ by keeping fixed values of G_1=0.1, G_2=0.1, R_e=0.2, m=0.1, L=0.2, δ=0.1, β=0.5, S^*_c=0.1, Γ_1=0.1, P_r=0.3, S_r=0.1, Γ_2=0.2 and N=0.3, E_1=0.1, E_2=0.2, M=0.1, φa*=0.3

Table 1: Total residual error of $\Phi(\Upsilon), \vartheta(\Upsilon), \varphi(\Upsilon)$ **and** $\zeta(\Upsilon)$ by keeping fixed values of G_1=0.1, G_2=0.1, R_e=0.2, m=0.1, L=0.2, δ=0.1, β=0.5, S^*_c=0.1, Γ_1=0.1, P_r=0.3, S_r=0.1, Γ_2=0.2, N=0.3, E_1=0.1, E_2=0.2, M=0.1, φ a*=0.3.

m	ε_ψ^{Φ}	$\varepsilon_\psi^{\vartheta}$	$\varepsilon_\psi^{\varphi}$	ε_ψ^{ζ}
1	0000023728	$2.34335*10^{-9}$	$3.38481*10^{-8}$	$1.97637*10^{-9}$
5	$3.94767*10^{-25}$	$7.31509*10^{-29}$	$7.00841*10^{-24}$	$4.07878*10^{-25}$
10	$1.45357*10^{-32}$	$2.32842*10^{-35}$	$2.18924*10^{-35}$	$2.5116*10^{-37}$
15	$1.55225*10^{-32}$	$2.518*10^{-35}$	$1.92443*10^{-35}$	$2.5116*10^{-37}$
20	$1.50295*10^{-32}$	$2.36453*10^{-35}$	$1.92443*10^{-35}$	$2.5116*10^{-37}$
25	$1.50295*10^{-32}$	$2.36453*10^{-35}$	$1.92443*10^{-35}$	$2.5116*10^{-37}$
30	$1.50295*10^{-32}$	$2.36453*10^{-35}$	$1.92443*10^{-35}$	$2.5116*10^{-37}$

35	$1.50295*10^{-32}$	$2.36453*10^{-35}$	$1.92443*10^{-35}$	$2.5116*10^{-37}$
40	$1.50295*10^{-32}$	$2.36453*10^{-35}$	$1.92443*10^{-35}$	$2.5116*10^{-37}$

Table 2: The Homotopy approach of convergence for various computational orders for $\Phi''(\Upsilon)$, $-\vartheta'(\Upsilon)$, $-\varphi'(\Upsilon)$, *and* $\text{Ç}'(\Upsilon)$, where keeping other parameters constant i.e. G_1=0.1, G_2=0.1, R_e=0.2, m=0.1, L=0.2, δ=0.1, β=0.5, S^*_c=0.5, Γ_1=0.1, P_r=0.5, S_r=0.3, Γ_2=0.5, N=0.5, E_1=0.1, E_2=0.2, M=0.3, φ a*=0.2.

	HAM results				Numerical results			
Υ	Φ''(0)	-ϑ'(0)	-φ'(0),	-Ç'(0)	Φ''(0)	-ϑ'(0)	-φ'(0),	-Ç'(0)
0	3.0048	1.0198	-0.1839	1.8394	3.0048	1.0198	-0.1839	1.8394
0.1001	2.3862	1.0203	-0.1880	1.8457	2.3862	1.0203	-0.1880	1.8457
0.2002	1.7822	1.0197	-0.1921	1.8557	1.7822	1.0197	-0.1921	1.8557
0.3003	1.1889	1.0177	-0.1960	1.8683	1.1889	1.0177	-0.1960	1.8683
0.4004	0.6016	1.0136	-0.1998	1.8825	0.6016	1.0136	-0.1998	1.8825
0.5005	0.0153	1.0073	-0.2032	1.8980	0.0153	1.0073	-0.2032	1.8980
0.6006	-0.5753	0.9988	-0.2063	1.9146	-0.5753	0.9988	-0.2063	1.9146
0.7007	-1.1757	0.9886	-0.2092	1.9325	-1.1757	0.9886	-0.2092	1.9325
0.8008	-1.7910	0.9774	-0.2118	1.9523	-1.7910	0.9774	-0.2118	1.9523
0.9009	-2.4263	0.9666	-0.2145	1.9750	-2.4263	0.9666	-0.2145	1.9750
1	-3.0796	0.9583	-0.2175	2.0019	-3.0796	0.9583	-0.2175	2.0019

Table 3: Computations for $\Phi(\Upsilon), \vartheta(\Upsilon), \varphi(\Upsilon)$ and $\text{Ç}(\Upsilon)$ when G_1=0.1, G_2=0.1, R_e=0.2, m=0.1, L=0.2, δ=0.1, β=0.5, S^*_c=0.5, Γ_1=0.1, P_r=0.5, S_r=0.5, Γ_2=0.5, N=0.5, E_1=0.1, E_2=0.2, M=0.3, φ a*=0.2. and different values of Υ.

	HAM results				Numerical results			
Υ	Φ(Υ)	ϑ(Υ)	φ(Υ)	Ç (Υ)	Φ(Υ)	ϑ(Υ)	φ(Υ)	Ç (Υ)
0	0	1.000	0.3679	1.9042	0	1.000	0.3679	1.9042
0.1001	0.0140	0.8979	0.4066	1.7198	0.0140	0.8979	0.4066	1.7198
0.2002	0.0520	0.7958	0.4494	1.5346	0.0520	0.7958	0.4494	1.5346
0.3003	0.1078	0.6938	0.4967	1.3482	0.1078	0.6938	0.4967	1.3482
0.4004	0.1755	0.5921	0.5490	1.1605	0.1755	0.5921	0.5490	1.1605
0.5005	0.2492	0.4909	0.6068	0.9713	0.2492	0.4909	0.6068	0.9713
0.6006	0.3231	0.3905	0.6707	0.7805	0.3231	0.3905	0.6707	0.7805
0.7007	0.3913	0.2910	0.7413	0.5880	0.3913	0.2910	0.7413	0.5880
0.8008	0.4476	0.1926	0.8194	0.3935	0.4476	0.1926	0.8194	0.3935
0.9009	0.4860	0.0954	0.9057	0.1970	0.4860	0.0954	0.9057	0.1970
1	05000	0	1.000	0	05000	0	1.000	0

6. Study of Results and Discussions on Graphs

We find and tabulate numerical solutions for the current flow problem over several fields with various dimensional parameters. The following section discusses observations made using plotted graphs of these data**.** The squeeze Reynolds number S_r, is the relationship among normal velocity of the upper plate and the kinematic viscosity of the fluid. It is essential to remember that large or small values of S_r, means that the slow or quick vertical velocity of an upper plate towards the lower plate. Positive values of S_r also indicates that the upper plate is moving towards the lower plate or a decrease in the distance among plates, whereas negative values of S_r indicates that the upper plate is moving away from the lower plate or a decreases in the distance among plates. The Figure 3 show the variation of S_r for velocity, which shows that by increasing squeezing number also cause of increasing of velocity profile. The squeezing velocity distribution Φ(Υ) is

observed for all potentially possible values of the Hartman number φa* in Figure 3. The resistive force acting between the particles is caused to act by the magnetic field, which outcomes in the reduced velocity. Including

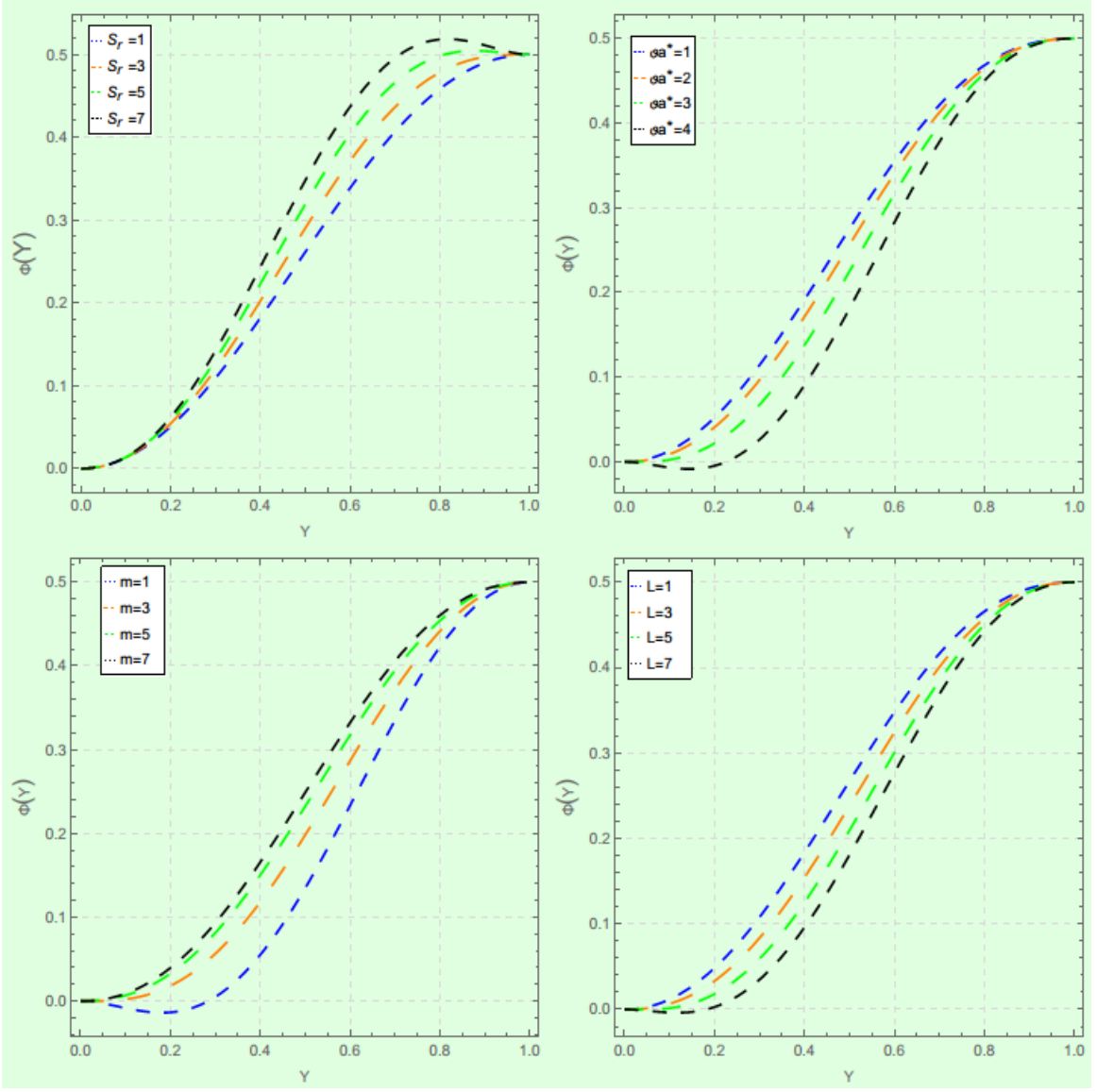

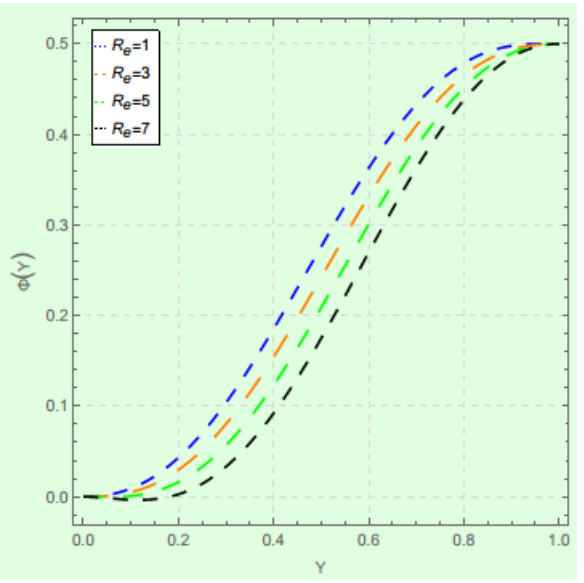

Figure 3: Variation of various parameters on velocity profile.

the Hall parameter results in a reduction in the amount of resistive force that is imposed by the magnetic field. due to its effect in reducing the effective conductivity. Hence, the velocity profile increases as the Hall parameter increases can be seen in figure 3. Increases in φa* therefore decrease velocity. The Reynolds number and Buoyancy number in figures 3 shows the same behavior for velocity profile like Hartman number. By increasing R_e and L causing of decreasing velocity profile. It is clear from fig. 4 that the squeezing of plates produced fluid friction, which causes of heat and this heat increases the temperature of fluid. Thus by increasing the squeezing parameter the temperature also increases. In the same way, Figures 4 show how the Prandtl number P_r affects temperature distribution profiles. Temperature profile is rises with increasing P_r as can be seen in Figure 4. Furthermore, it should be observed that decreasing values of P_r are linked to liquid materials that have small viscosity and high thermal conductivity, whereas increasing values of P_r are related with materials that have high viscosity, such as oils, and so on. Nevertheless, the flow region's dissipation effects are mostly to blame for the temperature profile increase. Moreover, heat dispersion occurs as a result of increased thermophoresis forces and as a conclusion, they cause of temperature rises. Additionally, the thickness of the thermal boundary layer decreases with the magnification values of P_r . Since by increases of prandtl number values causes of reduce the thickness of thermal boundary layer. Here by increases of porosity parameter the yield strength and compressive strength of the material will be increases.

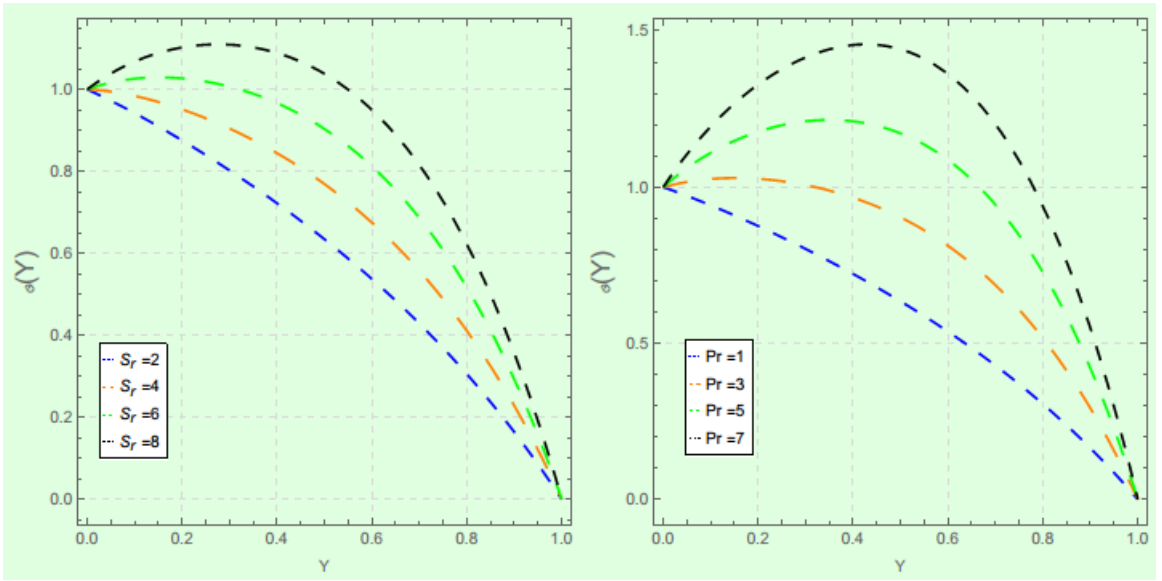

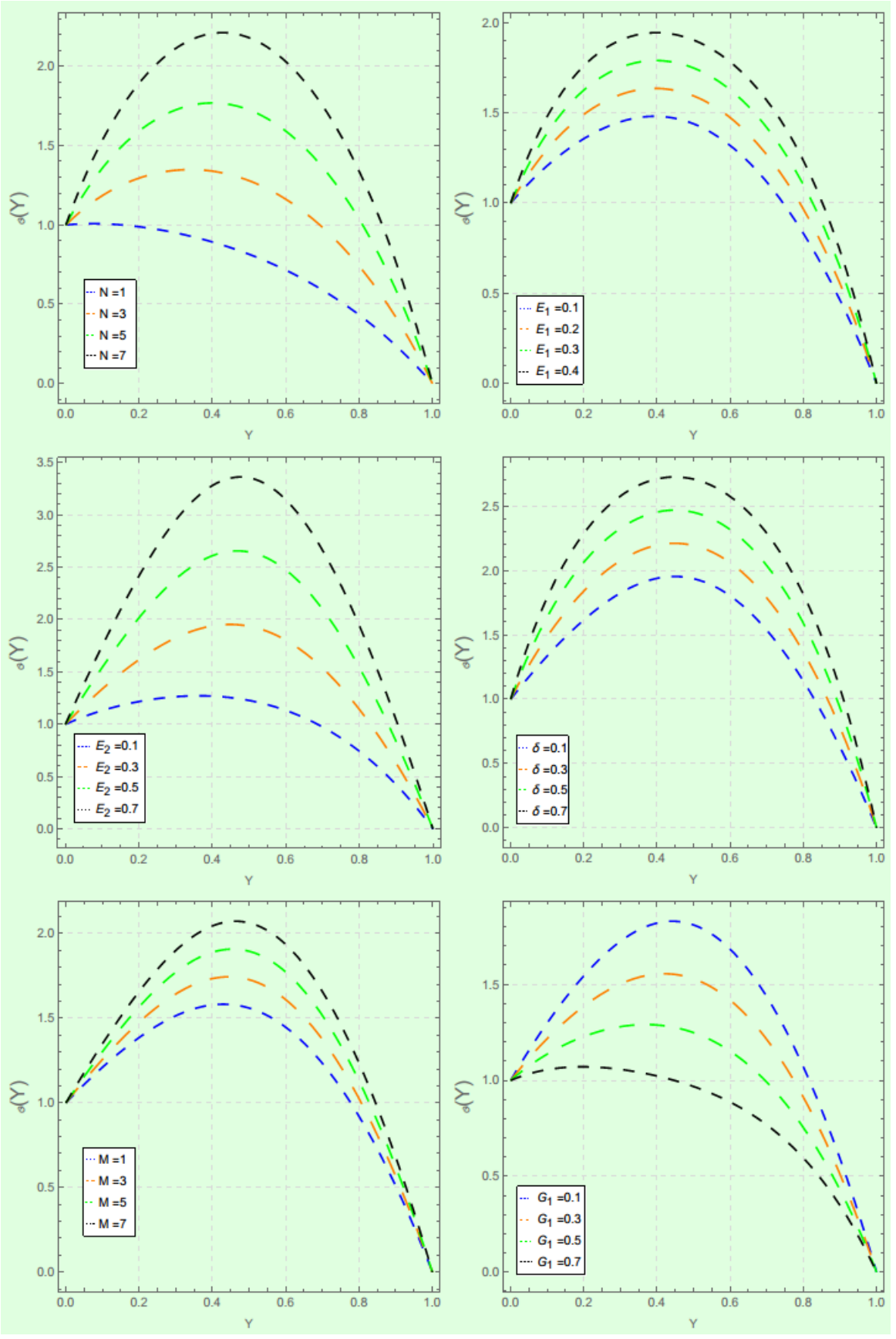
ϕ(Y)
Y
N =1
N =3
N =5
N =7
E_1 =0.1
E_1 =0.2
E_1 =0.3
E_1 =0.4
E_2 =0.1
E_2 =0.3
E_2 =0.5
E_2 =0.7
δ =0.1
δ =0.3
δ =0.5
δ =0.7
M =1
M =3
M =5
M =7
G_1 =0.1
G_1 =0.3
G_1 =0.5
G_1 =0.7

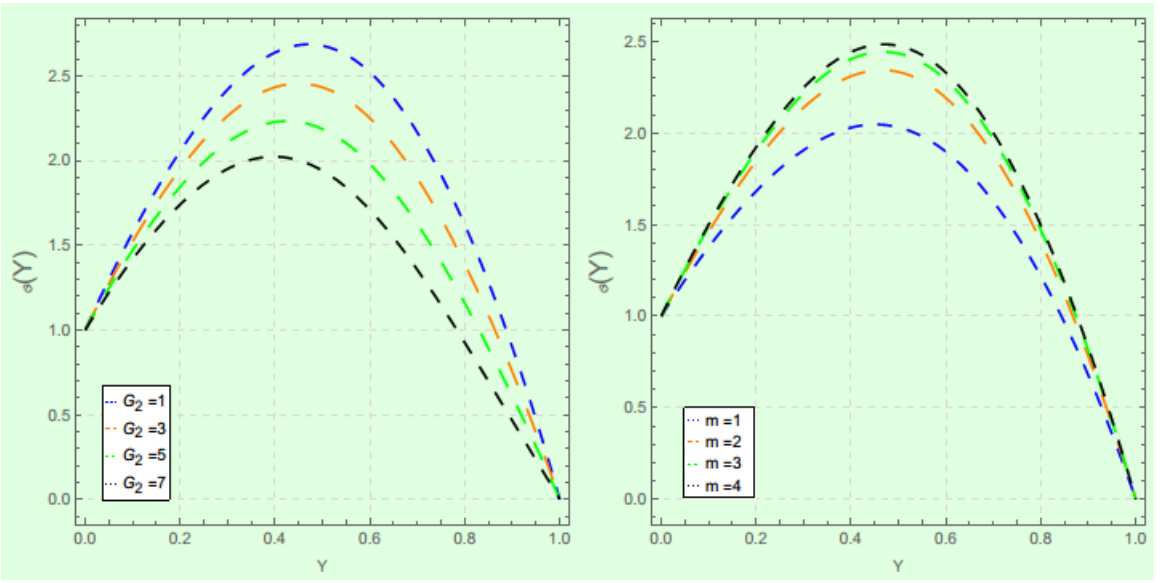

Figure 4: Variation of various parameters on Temperature distribution.

Figure 4 shows that the porosity parameter increasing with the increasing of the temperature distribution. As Eckret number shows the relationship of flow between kinetic energy and the boundary layer enthalpy difference and is expand to express heat dissipation. Figures 4 shows Eckret numbers E_1 and E_2 affect temperature profiles in the flow zone. Figures 4 illustrate that when E_1 and E_2 are magnified, the concentration profile falls and the thermal profile rises. Frictional and viscous dissipation effects are the cause of this. Figure 4 shows the effect of the temperature profile, with the increase of small parameter $\boldsymbol{\delta}$ increase with the temperature profile. The impact of the magnetic field parameter M on the temperature distribution profile inside the boundary layer is described in Figure 4. It is noticed that raising the magnetic field parameter M reduces velocity and raises temperature. In general, introducing a transverse magnetic field normal to the flow direction produces a flow-resistive force in the x direction. The fluid's upward travel along the plate is slowed down by this force in general. As a conclusion raises the temperature in the boundary layer. Consequently, the existence of a magnetic parameter produces a decrease in the rate of heat transmission at the surface. conversely, rising Grashof number G_1 and Brainkman number G_2 are affects temperature distribution shown in figures 4. The temperature drops as a result of the heat produced by this resistive force. Thus by increasing Grashof number and Brainkman number, the temperature distribution are decreasing.

Figure 4 shows that there is an increasing effect on temperature distribution as Hall parameter m increases. As we raise the rate of diffusion coefficient values, the Homogeneous reaction becomes slow due to decrease in the kinetic energy of particles. If the ambient temperature is lower, diffusion will occur more slowly. Decrease in temperature means that the decrease in molecules speed i.e (kinetic energy). As a result, the molecules move slower and the substance spreads less spontaneously, implying that diffusion happens at a slower rate. His effect can be seen in Figure 5. The variation of S_r is sketched in Figure 5. Here for larger S_r the homogeneous behavior increases. Behavior of $\boldsymbol{\Gamma_2}$ on Homogeneous behavior is illustrated in Figure 5. Here Homogeneous behavior decreases for higher values of $\boldsymbol{\Gamma_2}$. The variation of S^*_c is sketched in Figure 5. Here for larger S^*_c the homogeneous behavior increases. Figure 5 indicated an increase in the concentration distribution. The reason for the enhancement in concentration distribution is the decrease in the diffusion coefficient and the presence of fewer dispersed particles. It can be shown that schmidt number S^*_c increases the fluid's concentration diffusivity in Figure 5. It is because concentration decays due to greater diffusivity produced by increasing S^*_c. Due to the existence of a stronger homogeneous reaction, there is a reduction in the kinematic viscosity of the fluid, which leads to reduce the concentration profile. It is noticed that the concentration distribution is improved by the homogeneous chemical reaction parameter.

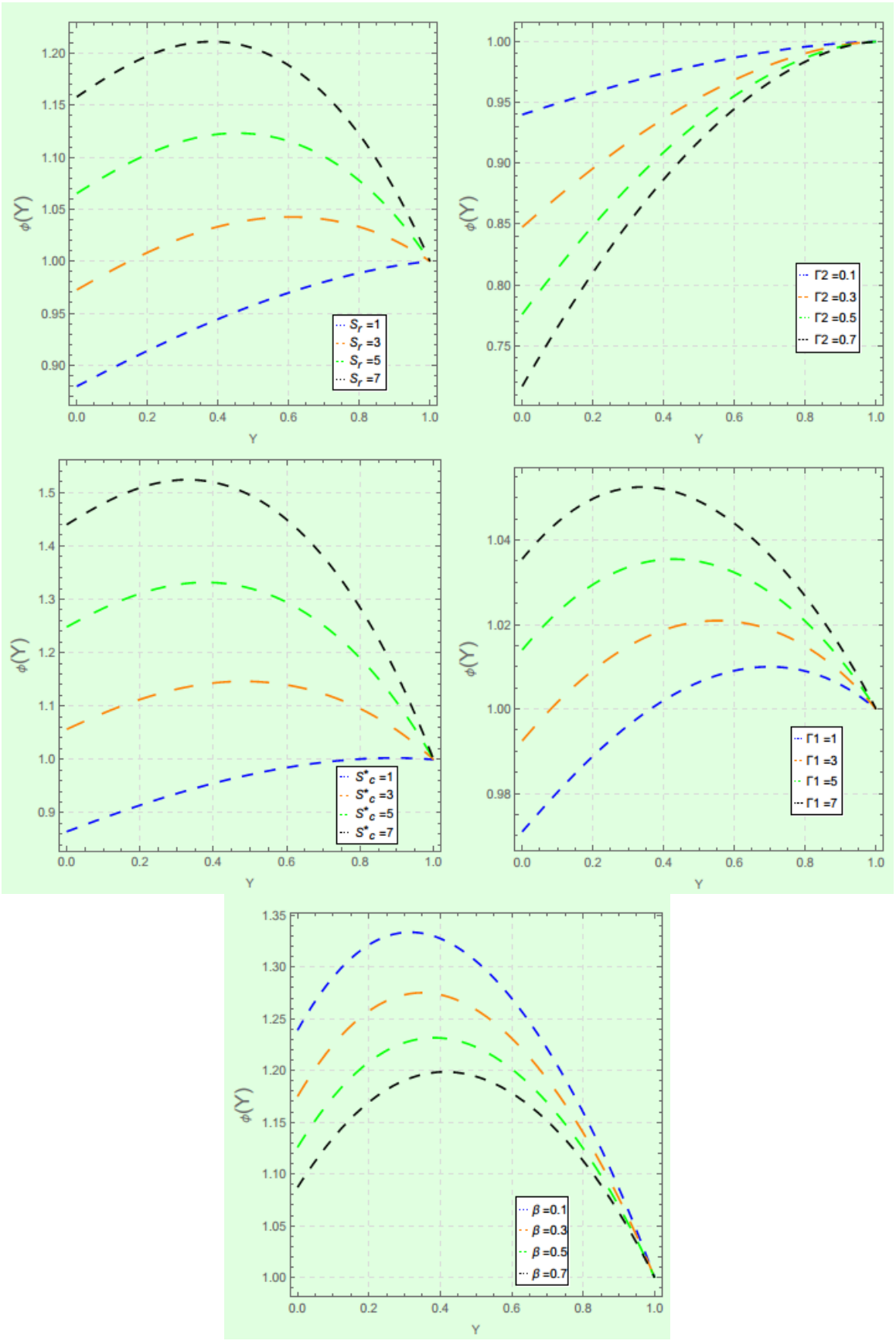

Figure 5: Variation of various parameters on Homogeneous chemical reaction.

Figure 5 shows that by increasing Γ_1 the homogeneous behavior increases. However the inverse variation can be seen in Figure 5 for parameter β. The heterogeneous behavior for S_r has been shown in Figure 6, which has an increasing effect on concentration. It is possible to properly manage the heat transmission from the surfaces of both plates by using temperature boundary conditions. The variation of S^*_c is sketched in Figure 6. Here for larger S^*_c the heterogeneous behavior increases. As for the equations to describe a heterogeneous reaction strength Γ_2 in Figures 6 and a homogeneous reaction strength Γ_1 in Figure 6 can be seen, respectively, illustrate the influence on the concentration profiles $\Phi(\Upsilon)$, $\varphi(\Upsilon)$ and $\text{Ǧ}(\Upsilon)$. It is noticed that a rise in Γ_1 is responsible for the concentration profiles $\Phi(\Upsilon)$, $\varphi(\Upsilon)$ and $\text{Ǧ}(\Upsilon)$. This indicates a decrease in viscosity due to raise in the homogeneous chemical reaction parameter. The concentration for β will drop primly then shows the increasing behavior shown in Figure 6. 3D variation of $\Phi(\Upsilon), \vartheta(\Upsilon), \varphi(\Upsilon)$ and $\text{Ǧ}(\Upsilon)$ by keeping various parameters constants are shown in Figures 7.

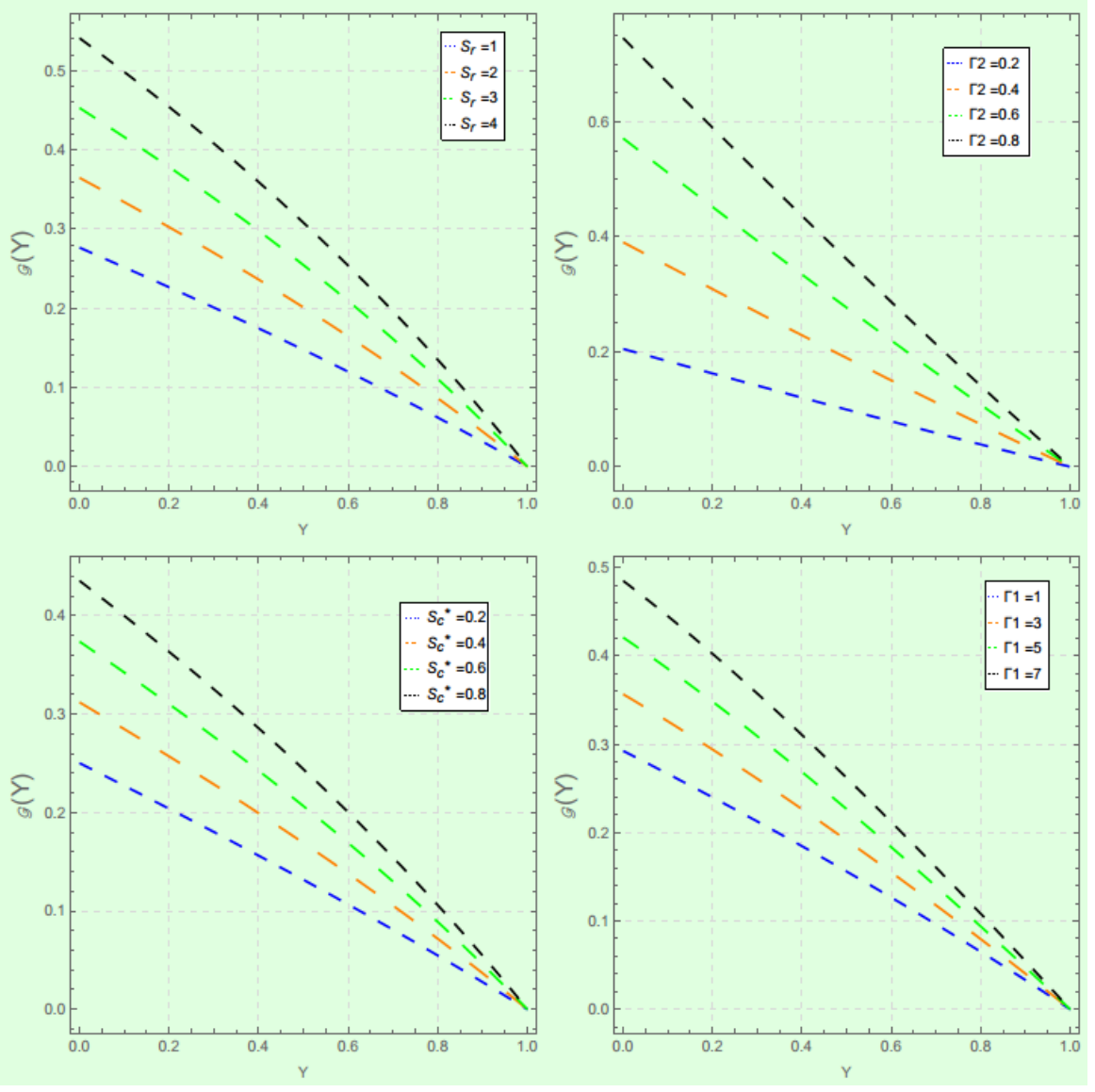

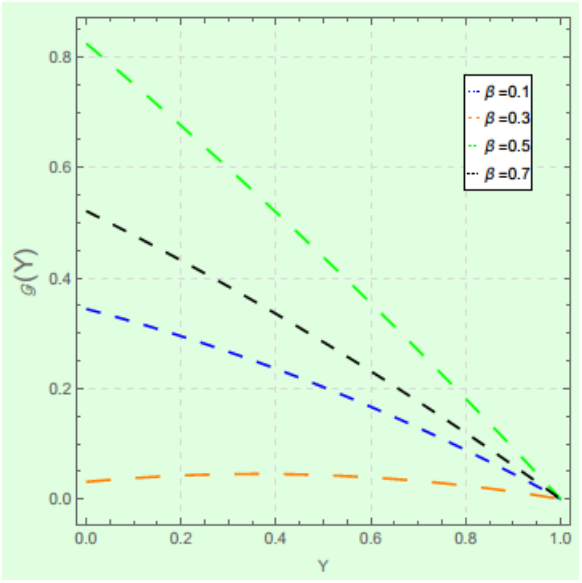

Figure 6: Variation of various parameters on Heterogeneous chemical reaction.

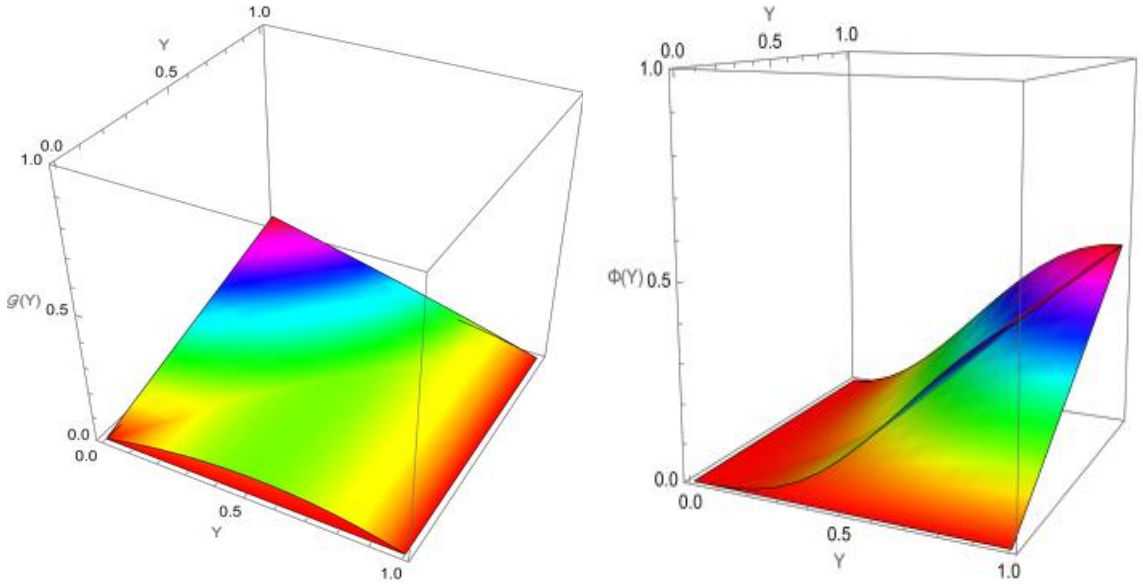

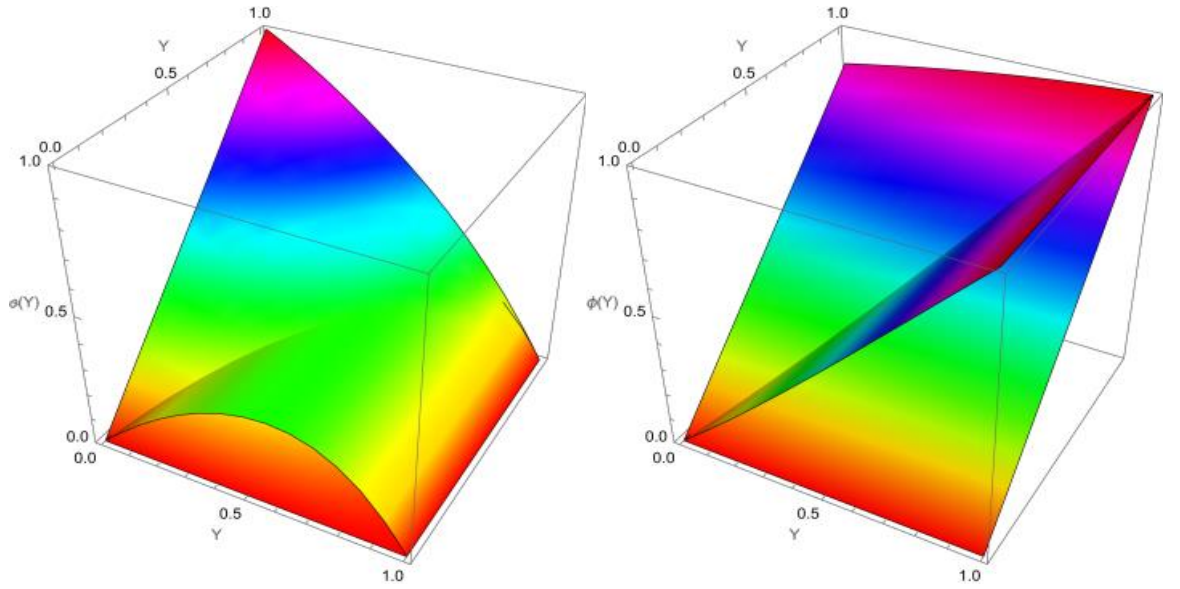

Figure 7: 3D variation of $\Phi(\Upsilon), \vartheta(\Upsilon), \varphi(\Upsilon)$ and $Ģ(\Upsilon)$.

7. Discussion on Numerical Results

Tables (4–17) are designed to investigate the effects of different specific parameters numerically. The provided tables show that there is great agreement between all consequences and the results obtained using BVP4c and HAM. The effects of temperature, velocity and both homogeneous and heterogeneous characteristics are observed to have a propensity to raise the rate of mass transfer. Although, it does not show a significant shift in the rate of heat transfer and friction factor. Increased internal heat production reduces both the heat transfer rate and the skin friction coefficient. The raise in the squeeze parameter S_r has yielded comparable results for us. Reduces the friction factor by raising the squeezing number S_r whereas raising the Sherwood and Nusselt numbers locally. In this instance, the coefficient of skin friction display a negative direction, indicating that the fluid is being pulled by the surface. The effects of the following parameters are displayed in Tables (4–17): $\Phi''(\Upsilon)$, $-\vartheta'(\Upsilon)$, $-\varphi'(\Upsilon)$, *and* $Ģ'(\Upsilon)$ each. It can be seen that, for growing parameters S_r and P^*_r, the magnitude of the momentum transfer coefficient increases in tables (4-5), whereas for rising values of N, it reduce in table (6).

Tables (7) show a result that by increasing parameter β the $-Ģ'(0)$ decreasing. As the values of the parameters E_1 and E_2 raises, shows that the effect on temperature distribution is to decreases shown in tables (8-9). Since the Eckret number typically serves to quantify the effect of Joule heating, table (8-9) are constructed to display the temperature distributions for constructed Eckret number values. It has been noted that when the Eckert number increases, the thickness of the thermal boundary layer reduces.

Table 4: Working with calculations for $\Phi''(0)$, $-\vartheta'(0)$, $-\varphi'(0)$, and $-Ģ'(0)$ when G_1=0.1, G_2=0.1, R_e=0.2, m=0.1, L=0.2, δ=0.1, β=0.5, S^*_c=0.5, Γ_1=0.1, S_r=0.3, Γ_2=0.5, N=0.5, E_1=0.1, E_2=0.2, M=0.3, φ a*=0.2. by different values of P_r.

	HAM results				Numerical results			
P_r	$\Phi''(0)$	$-\vartheta'(0)$	$-\varphi'(0)$	$-Ģ'(0)$	$\Phi''(0)$	$-\vartheta'(0)$	$-\varphi'(0)$	$-Ģ(0)$
0.5	3.0048	1.0198	-0.1839	1.8394	3.0048	1.0198	-0.1839	1.8394
0.7	3.0048	1.0278	-0.1839	1.8394	3.0048	1.0278	-0.1839	1.8394
0.9	3.0048	1.0357	-0.1839	1.8394	3.0048	1.0357	-0.1839	1.8394
1.1	3.0048	1.0436	-0.1839	1.8394	3.0048	1.0436	-0.1839	1.8394

Table 5: Working with calculations for $\Phi''(0)$, $-\vartheta'(0)$, $-\varphi'(0)$, and $-G'(0)$ when $G_1=0.1$, $G_2=0.1$, $R_e=0.2$, m=0.1, L=0.2, $\delta=0.1$, $\beta=0.5$, $S^*_c=0.5$, $\Gamma_1=0.1$, $P_r=0.5$, $\Gamma_2=0.5$, N=0.5, $E_1=0.1$, $E_2=0.2$, M=0.3, φ a*=0.2. by different values of S_r

	HAM results				Numerical results			
S_r	$\Phi''(0)$	$-\vartheta'(0)$	$-\varphi'(0)$	$-G'(0)$	$\Phi''(0)$	$-\vartheta'(0)$	$-\varphi'(0)$	$-G(0)$
0.1	3.0017	1.0066	-0.1839	1.8394	3.0017	1.0066	-0.1839	1.8394
0.2	3.0032	1.0132	-0.1839	1.8394	3.0032	1.0132	-0.1839	1.8394
0.3	3.0048	1.0198	-0.1839	1.8394	3.0048	1.0198	-0.1839	1.8394
0.4	3.0065	1.0264	-0.1839	1.8394	3.0065	1.0264	-0.1839	1.8394

Table 6: Working with calculations for $\Phi''(0)$, $-\vartheta'(0)$, $-\varphi'(0)$, and $-G'(0)$ when $G_1=0.1$, $G_2=0.1$, $R_e=0.2$, m=0.1, L=0.2, $\delta=0.1$, $\beta=0.5$, $S^*_c=0.5$, $\Gamma_1=0.1$, $P_r=0.5$, $S_r=0.3$, $\Gamma_2=0.5$, $E_1=0.1$, $E_2=0.2$, M=0.3, φ a*=0.2. by different values of N.

	HAM results				Numerical results			
N	$\Phi''(0)$	$-\vartheta'(0)$	$-\varphi'(0)$	$-G'(0)$	$\Phi''(0)$	$-\vartheta'(0)$	$-\varphi'(0)$	$-G(0)$
0.5	3.0048	1.0198	-0.1839	1.8394	3.0048	1.0198	-0.1839	1.8394
1	3.0048	1.0143	-0.1839	1.8394	3.0048	1.0143	-0.1839	1.8394
1.5	3.0048	1.0087	-0.1839	1.8394	3.0048	1.0087	-0.1839	1.8394
2	3.0048	1.0031	-0.1839	1.8394	3.0048	1.0031	-0.1839	1.8394

Table 7: Working with calculations for $\Phi''(0)$, $-\vartheta'(0)$, $-\varphi'(0)$, and $-G'(0)$ when $G_1=0.1$, $G_2=0.1$, $R_e=0.2$, m=0.1, L=0.2, $\delta=0.1$, $S^*_c=0.5$, $\Gamma_1=0.1$, $P_r=0.5$, $S_r=0.3$, $\Gamma_2=0.5$, $E_1=0.1$, $E_2=0.2$, M=0.3, φ a*=0.2, N=0.5,. by different values of β.

	HAM results				Numerical results			
β	$\Phi''(0)$	$-\vartheta'(0)$	$-\varphi'(0)$	$-G'(0)$	$\Phi''(0)$	$-\vartheta'(0)$	$-\varphi'(0)$	$-G(0)$
0.1	3.0065	1.0159	-0.1839	1.8394	3.0065	1.0159	-0.1839	1.8394
0.2	3.0065	1.0159	-0.1839	0.9197	3.0065	1.0159	-0.1839	0.9197
0.3	3.0065	1.0159	-0.1839	0.6131	3.0065	1.0159	-0.1839	0.6131
0.4	3.0065	1.0159	-0.1839	0.4598	3.0065	1.0159	-0.1839	0.4598

Table 8: Working with calculations for $\Phi''(0)$, $-\vartheta'(0)$, $-\varphi'(0)$, and $-G'(0)$ when $G_1=0.1$, $G_2=0.1$, $R_e=0.2$, m=0.1, L=0.2, $\delta=0.1$, $S^*_c=0.5$, $\Gamma_1=0.1$, $P_r=0.5$, $S_r=0.3$, $\Gamma_2=0.5$, $\beta=0.1$, $E_2=0.2$, M=0.3, φ a*=0.2, N=0.5,. by different values of E_1.

	HAM results				Numerical results			

E_1	$\Phi''(0)$	$-\vartheta'(0)$	$-\varphi'(0)$	$-\text{Ç}'(0)$	$\Phi''(0)$	$-\vartheta'(0)$	$-\varphi'(0)$	$-\text{Ç}(0)$
0.1	3.0065	1.0159	-0.1839	1.8394	3.0065	1.0159	-0.1839	1.8394
0.3	3.0065	1.0141	-0.1839	1.8394	3.0065	1.0141	-0.1839	1.8394
0.5	3.0065	1.0123	-0.1839	1.8394	3.0065	1.0123	-0.1839	1.8394
0.7	3.0065	1.0105	-0.1839	1.8394	3.0065	1.0105	-0.1839	1.8394

Table 9: Working with calculations for $\Phi''(0)$, $-\vartheta'(0)$, $-\varphi'(0)$, and $-\text{Ç}'(0)$ when $G_1=0.1$, $G_2=0.1$, $R_e=0.2$, m=0.1, L=0.2, $\delta=0.1$, $S^*_c=0.5$, $\Gamma_1=0.1$, $P_r=0.5$, $S_r=0.3$, $\Gamma_2=0.5$, $\beta=0.1$, $E_1=0.1$, M=0.3, φ a*=0.2, N=0.5,. by different values of E_2.

	HAM results				Numerical results			
E_2	$\Phi''(0)$	$-\vartheta'(0)$	$-\varphi'(0)$	$-\text{Ç}'(0)$	$\Phi''(0)$	$-\vartheta'(0)$	$-\varphi'(0)$	$-\text{Ç}(0)$
0.1	3.0065	1.0177	-0.1839	1.8394	3.0065	1.0177	-0.1839	1.8394
0.3	3.0065	1.0141	-0.1839	1.8394	3.0065	1.0141	-0.1839	1.8394
0.5	3.0065	1.0105	-0.1839	1.8394	3.0065	1.0105	-0.1839	1.8394
0.7	3.0065	1.0069	-0.1839	1.8394	3.0065	1.0069	-0.1839	1.8394

Table 10: Working with calculations for $\Phi''(0)$, $-\vartheta'(0)$, $-\varphi'(0)$, and $-\text{Ç}'(0)$ when $G_1=0.1$, $G_2=0.1$, $R_e=0.2$, m=0.1, L=0.2, $\delta=0.1$, $E_2=0.2$, $\Gamma_1=0.1$, $P_r=0.5$, $S_r=0.3$, $\Gamma_2=0.5$, $\beta=0.1$, $E_1=0.1$, M=0.3, φ a*=0.2, N=0.5,. by different values of S^*_c.

	HAM results				Numerical results			
S^*_c	$\Phi''(0)$	$-\vartheta'(0)$	$-\varphi'(0)$	$-\text{Ç}'(0)$	$\Phi''(0)$	$-\vartheta'(0)$	$-\varphi'(0)$	$-\text{Ç}(0)$
0.1	3.0065	1.0159	-0.1839	1.8394	3.0065	1.0159	-0.1839	1.8394
1	28917	0.6441	-0.0368	0.1226	28917	0.6441	-0.0368	0.1226
2	28917	0.6441	-0.0368	0.1226	28917	0.6441	-0.0368	0.1226
4	28917	0.6441	-0.0368	0.1226	28917	0.6441	-0.0368	0.1226

Table 11: Working with calculations for $\Phi''(0)$, $-\vartheta'(0)$, $-\varphi'(0)$, and $-\text{Ç}'(0)$ when $G_1=0.1$, $G_2=0.1$,, m=0.1, L=0.2, $S^*_c=0.5$, $\delta=0.1$, $E_2=0.2$, $\Gamma_1=0.1$, $P_r=0.5$, $S_r=0.3$, $\Gamma_2=0.5$, $\beta=0.1$, $E_1=0.1$, M=0.3, φ a*=0.2, N=0.5,. by different values of R_e.

	HAM results				Numerical results			
R_e	$\Phi''(0)$	$-\vartheta'(0)$	$-\varphi'(0)$,	$-\text{Ç}'(0)$	$\Phi''(0)$	$-\vartheta'(0)$	$-\varphi'(0)$,	$-\text{Ç}'(0)$
0.1	3.0065	1.0159	-0.1839	1.8394	3.0065	1.0159	-0.1839	1.8394
2.8	3.0066	1.0159	-0.0368	1.8394	3.0066	0.6441	-0.0368	1.8394
7	3.0067	1.0159	-0.0368	1.8394	3.0067	0.6441	-0.0368	1.8394
12	3.0068	1.0159	-0.0368	1.8394	3.0068	0.6441	-0.0368	1.8394

Table 12: Working with calculations for $\Phi''(0)$, $-\vartheta'(0)$, $-\varphi'(0)$, and $-\text{Ç}'(0)$ when $G_1=0.1$, $G_2=0.1$,, m=0.1, L=0.2, $S^*_c=0.5$, $\delta=0.1$, $E_2=0.2$, $\Gamma_1=0.1$, $P_r=0.5$, $S_r=0.3$, $\Gamma_2=0.5$, $\beta=0.1$, $E_1=0.1$, M=0.3, $R_e=0.2$, N=0.5,. by different values of φ a*

	HAM results				Numerical results			
φ a*	$\Phi''(0)$	$-\vartheta'(0)$	$-\varphi'(0)$,	$-\text{Ç}'(0)$	$\Phi''(0)$	$-\vartheta'(0)$	$-\varphi'(0)$,	-

								$-G'(0)$
0.2	3.0065	1.0159	-0.1839	1.8394	3.0065	1.0159	-0.1839	1.8394
1.4	3.0163	1.0159	-0.1839	1.8394	3.0163	1.0159	-0.1839	1.8394
2.2	3.0308	1.0159	-0.1839	1.8394	3.0308	1.0159	-0.1839	1.8394
3.2	3.0579	1.0159	-0.1839	1.8394	3.0579	1.0159	-0.1839	1.8394

Table 13: Working with calculations for $\Phi''(0)$, $-\vartheta'(0)$, $-\varphi'(0)$, and $-G'(0)$ when $G_1=0.1$, $G_2=0.1$,, m=0.1, L=0.2, $S^*_c=0.5$, $\delta=0.1$, $E_2=0.2$, $\Gamma_1=0.1$, $P_r=0.5$, $S_r=0.3$, $\Gamma_2=0.5$, $\beta=0.1$, $E_1=0.1$, φ a*=0.2, $R_e=0.2$, N=0.5,. by different values of M

	HAM results				Numerical results			
M	$\Phi''(0)$	$-\vartheta'(0)$	$-\varphi'(0)$	$-G'(0)$	$\Phi''(0)$	$-\vartheta'(0)$	$-\varphi'(0)$	$-G(0)$
0.3	3.0065	1.0159	-0.1839	1.8394	3.0065	1.0159	-0.1839	1.8394
0.7	3.0065	1.0151	-0.1839	1.8394	3.0065	1.0151	-0.1839	1.8394
1.2	3.0065	1.0141	-0.1839	1.8394	3.0065	1.0141	-0.1839	1.8394
1.6	3.0065	1.0132	-0.1839	1.8394	3.0065	1.0132	-0.1839	1.8394

Table 14: Working with calculations for $\Phi''(0)$, $-\vartheta'(0)$, $-\varphi'(0)$, and $-G'(0)$ when $G_1=0.1$, $G_2=0.1$,, m=0.1, M=0.3, $S^*_c=0.5$, $\delta=0.1$, $E_2=0.2$, $\Gamma_1=0.1$, $P_r=0.5$, $S_r=0.3$, $\Gamma_2=0.5$, $\beta=0.1$, $E_1=0.1$, φ a*=0.2, $R_e=0.2$, N=0.5,. by different values of L

	HAM results				Numerical results			
L	$\Phi''(0)$	$-\vartheta'(0)$	$-\varphi'(0)$	$-G'(0)$	$\Phi''(0)$	$-\vartheta'(0)$	$-\varphi'(0)$	$-G(0)$
0.1	3.0065	1.0159	-0.1839	1.8394	3.0065	1.0159	-0.1839	1.8394
0.3	3.0069	1.0159	-0.1839	1.8394	3.0069	1.0159	-0.1839	1.8394
0.5	3.0073	1.0159	-0.1839	1.8394	3.0073	1.0159	-0.1839	1.8394
0.7	3.0078	1.0159	-0.1839	1.8394	3.0078	1.0159	-0.1839	1.8394

Table 15: Working with calculations for $\Phi''(0)$, $-\vartheta'(0)$, $-\varphi'(0)$, and $-G'(0)$ when L=0.2, $G_2=0.1$,, m=0.1, M=0.3, $S^*_c=0.5$, $\delta=0.1$, $E_2=0.2$, $\Gamma_1=0.1$, $P_r=0.5$, $S_r=0.3$, $\Gamma_2=0.5$, $\beta=0.1$, $E_1=0.1$, φ a*=0.2, $R_e=0.2$, N=0.5,. by different values of G_1

	HAM results				Numerical results			
G_1	$\Phi''(0)$	$-\vartheta'(0)$	$-\varphi'(0)$	$-G'(0)$	$\Phi''(0)$	$-\vartheta'(0)$	$-\varphi'(0)$	$-G(0)$
0.1	3.0067	1.0159	-0.1839	1.8394	3.0067	1.0159	-0.1839	1.8394
0.3	3.0067	1.0148	-0.1839	1.8394	3.0067	1.0148	-0.1839	1.8394
0.5	3.0067	1.0137	-0.1839	1.8394	3.0067	1.0137	-0.1839	1.8394
0.7	3.0067	1.0127	-0.1839	1.8394	3.0067	1.0127	-0.1839	1.8394

Table 16: Working with calculations for $\Phi''(0)$, $-\vartheta'(0)$, $-\varphi'(0)$, and $-\text{Ç}'(0)$ when L=0.2, G_1=0.1,, m=0.1, M=0.3, S^*_c=0.5, δ=0.1, E_2=0.2, Γ_1=0.1, P_r =0.5, S_r=0.3, Γ_2=0.5, β=0.1, E_1=0.1, φ a*=0.2, R_e =0.2, N=0.5,. by different values of G_2

	HAM results				Numerical results			
G_2	$\Phi''(0)$	$-\vartheta'(0)$	$-\varphi'(0)$	$-\text{Ç}'(0)$	$\Phi''(0)$	$-\vartheta'(0)$	$-\varphi'(0)$	$-\text{Ç}(0)$
0.1	3.0067	1.0159	-0.1839	1.8394	3.0067	1.0159	-0.1839	1.8394
0.2	3.0067	1.0158	-0.1839	1.8394	3.0067	1.0158	-0.1839	1.8394
0.3	3.0067	1.0157	-0.1839	1.8394	3.0067	1.0157	-0.1839	1.8394
0.4	3.0067	1.0156	-0.1839	1.8394	3.0067	1.0156	-0.1839	1.8394

Table 17: Working with calculations for $\Phi''(0)$, $-\vartheta'(0)$, $-\varphi'(0)$, and $-\text{Ç}'(0)$ when L=0.2, G_1=0.1,, G_2=0.1, M=0.3, S^*_c=0.5, δ=0.1, E_2=0.2, Γ_1=0.1, P_r =0.5, S_r=0.3, Γ_2=0.5, β=0.1, E_1=0.1, φ a*=0.2, R_e =0.2, N=0.5,. by different values of m

	HAM results				Numerical results			
m	$\Phi''(0)$	$-\vartheta'(0)$	$-\varphi'(0)$	$-\text{Ç}'(0)$	$\Phi''(0)$	$-\vartheta'(0)$	$-\varphi'(0)$	$-\text{Ç}(0)$
0.1	3.0067	1.0159	-0.1839	1.8394	3.0067	1.0159	-0.1839	1.8394
0.5	3.0067	1.0160	-0.1839	1.8394	3.0067	1.0160	-0.1839	1.8394
1	3.0067	1.0162	-0.1839	1.8394	3.0067	1.0162	-0.1839	1.8394
2	3.0067	1.0164	-0.1839	1.8394	3.0067	1.0164	-0.1839	1.8394

The variation of S^*_c is shown in table 10. Here for larger S^*_c the homogeneous behavior increases, whereas the velocity profile, temperature distribution and heterogeneous reaction are all decreasing. Table 10 indicated an increase in the concentration distribution. The reason for the enhancement in concentration distribution is the decrease in the diffusion coefficient and the presence of fewer dispersed particles. It can be shown that schmidt number S^*_c increases the fluid's concentration diffusivity. It is because concentration decays due to greater diffusivity produced by increasing S^*_c

Tables (11) show a result for Reynolds number that by increasing parameter R_e the smoothly increasing. Whereas the Hartman number, convection parameter also show that in table (12,14) that increasing it, the velocity profile increases.

It is observed that in tables (13, 15, 16) temperature distribution decreases with increasing the parameters M, G_1 and G_2. An increase in M is observed to cause a reduction in the temperature profile, which is caused by the Lorentz force. Additionally, it is well known that a bigger magnetic parameter results in a stronger Lorentz force, which raises temperature and forms a thicker thermal boundary layer. The temperature and concentration profile rise as a conclusion of that aspect. However, when considering with enhancing Hall parameter m as a result of reducing the velocity and increasing temperature shown in table 17.

8. Conclusions

The flow in presence of Hall current and viscous dissipation with both homogeneous and heterogeneous reactions between two squeezing plates are considered in this research paper along with the numerical solution have been analysed. Together with the skin friction factor, Sherwood numbers and local Nusselt number, graphs and tables are utilized to show and explain the impacts of non-dimensional leading arguments on velocity, viscous and joule heating dissipation, and homogeneous/heterogeneous profiles. Following are the conclusions of current investigation;

- With rising values of the Hall parameter m, porosity parameter N, and magnetic parameter M, the velocity field and temperature profile both increase.
- It is evident that the velocity field increases as S_r increases. In actuality, increasing the amount of pressure applied to the fluid reduces its kinematic viscosity, which lowers fluid velocity.
- The behaviour of flow with the Hartman number φa*, the normal velocity profile decreases for the enhancing φa* levels. Greater resistance to the flow results from larger Lorentz forces, which causes the velocity field to decrease.
- The velocity and temperature profiles decreases for increasing the Groshof parameter G_1, Brainkman number G_2, Reynolds number and convection parameter.
- The temperature profile's response to the prandtl number P_r is illustrated as, because P_r express the ratio of the viscous diffusion rate to the thermal diffusion rate, greater prandtl number values result in lower thermal diffusivity. The temperature profiles thus increase as P_r rises.
- Temperature distributions for contracting Eckert number values yields a general description of the Joule heating effect, denoted as E_1 and E_2, respectively. When the Eckert number increases, it was established that the thickness of the thermal boundary layer and the volume percentage of nano-particles both rise. This occurs as a result of viscous dissipation, which heats the regime by acting as an internal heat source and raising thermal energy in the energy equation.

9. Nomenclature

μ	Dynamic viscosity
p	Pressure of fluid
ρ	Effective density
C_p	Specific heat capacity
σ	Electrical conductivity
Ψ, ν	Velocity components
φ	Temperature distribution
ϕ_l, ϕ_u	Temperature of upper and lower plates
D_Ω, D_B *	Diffusion coefficients of the chemical species
β	Ratio of the diffusion coefficients
Γ_1	Homogeneous reaction strength
Γ_2	Heterogeneous reaction strength
S_r	Squeeze Reynolds number
P_{r_*}	Prandtl number
φa^*	Hartman number
C_f	Skin-friction coefficient
N_u	Local Nusselt number
S_h	Sherwood number
Ω_1, Ω_2	Chemical species
E_1	Local Eckert number
E_2	Eckret number
M	Magnetic field parameter
S^*_c	Schmidth number
L	Convection or buoyancy parameter
R_e	Reynolds number
G_1	Grashof number
G_2	Brainkman number
m	Hall parameter
δ	Small parameter
N	Porosity number

Acknowledgment

This Project was funded by the Deanship of Scientific Research (DSR) at King Abdulaziz University, Jeddah, under grant no. (GPIP: 1434–305–2024). The authors, therefore, acknowledge with thanks DSR for technical and financial support.

References

[1] M. Stefan, Versuch Uber die scheinbare adhesion, Akademie der Wissenschaften in Wien. vol. 69, Mathematik-Naturwissen, 1874.

[2] X. Ran, Q. Zhu, Y. Li, An explicit series solution of the squeezing flow between two infinite plates by means of the homotopy analysis method, *Communications in Nonlinear Science and Numerical Simulation,* Vol. 14, No. 1, pp. 119-132, 2009.

[3] M. Mustafa, T. Hayat, S. Obaidat, On heat and mass transfer in the unsteady squeezing flow between parallel plates, *Meccanica,* Vol. 47, No. 7, pp. 1581-1589, 2012.

[4] M. Sheikholeslami, M. B. Gerdroodbary, R. Moradi, A. Shafee, Z. Li, Application of Neural Network for estimation of heat transfer treatment of Al2O3-H2O nanofluid through a channel, *Computer Methods in Applied Mechanics and Engineering,* Vol. 344, pp. 1-12, 2019.

[5] T. Hayat, M. Khan, M. Imtiaz, A. Alsaedi, Squeezing flow past a Riga plate with chemical reaction and convective conditions, *Journal of Molecular Liquids,* Vol. 225, pp. 569-576, 2017.

[6] S. Ahmad, M. Farooq, M. Javed, A. Anjum, Slip analysis of squeezing flow using doubly stratified fluid, *Results in Physics,* Vol. 9, pp. 527-533, 2018.

[7] T. Hayat, F. Haider, T. Muhammad, A. Alsaedi, Darcy–Forchheimer squeezed flow of carbon nanotubes with thermal radiation, *Journal of Physics and Chemistry of Solids,* Vol. 120, pp. 79-86, 2018.

[8] S. Ahmad, M. Farooq, M. Javed, A. Anjum, Double stratification effects in chemically reactive squeezed Sutterby fluid flow with thermal radiation and mixed convection, *Results in physics,* Vol. 8, pp. 1250-1259, 2018.

[9] R. Cortell, Fluid flow and radiative nonlinear heat transfer over a stretching sheet, *Journal of King Saud University-Science,* Vol. 26, No. 2, pp. 161-167, 2014.

[10] S. A. Shehzad, T. Hayat, A. Alsaedi, M. A. Obid, Nonlinear thermal radiation in three-dimensional flow of Jeffrey nanofluid: a model for solar energy, *Applied Mathematics and Computation,* Vol. 248, pp. 273-286, 2014.

[11] M. Mustafa, A. Mushtaq, T. Hayat, B. Ahmad, Nonlinear radiation heat transfer effects in the natural convective boundary layer flow of nanofluid past a vertical plate: a numerical study, *PLoS One,* Vol. 9, No. 9, pp. e103946, 2014.

[12] J. Hartmann, F. Lazarus, 1937, *Experimental investigations on the flow of mercury in a homogeneous magnetic field*, Munksgaard,

[13] L. Tao, Magnetohydrodynamic effects on the formation of Couette flow, *Journal of the Aerospace Sciences,* Vol. 27, No. 5, pp. 334-338, 1960.

[14] R. Alpher, Heat transfer in magnetohydrodynamic flow between parallel plates, *International Journal of Heat and Mass Transfer,* Vol. 3, No. 2, pp. 108-112, 1961.

[15] G. W. Sutton, A. Sherman, 2006, *Engineering magnetohydrodynamics*, Courier Dover Publications,

[16] K. R. Cramer, S.-I. Pai, Magnetofluid dynamics for engineers and applied physicists, 1973.

[17] S. Nigam, S. Singh, Heat transfer by laminar flow between parallel plates under the action of transverse magnetic field, *The Quarterly Journal of Mechanics and Applied Mathematics,* Vol. 13, No. 1, pp. 85-97, 1960.

[18] H. A. Attia, N. Kotb, MHD flow between two parallel plates with heat transfer, *Acta mechanica,* Vol. 117, No. 1, pp. 215-220, 1996.

[19] I. Tani, Steady flow of conducting fluids in channels under transverse magnetic fields, with consideration of Hall effect, *Journal of the Aerospace Sciences,* Vol. 29, No. 3, pp. 297-305, 1962.

[20] V. Soundalgekar, N. Vighnesam, H. Takhar, Hall and ion-slip effects in MHD Couette flow with heat transfer, *IEEE Transactions on Plasma Science,* Vol. 7, No. 3, pp. 178-182, 2007.

[21] V. Soundalgekar, A. Uplekar, Hall effects in MHD Couette flow with heat transfer, *IEEE Transactions on Plasma Science,* Vol. 14, No. 5, pp. 579-583, 1986.

[22] E. Abo-El-Dahab, Effect of Hall currents on some magnetohydrodynamic flow problems, *Master's Thesis, Department of Maths, Faculty of Science, Helwan University, Egypt*, 1993.

[23] H. A. Attia, Hall current effects on the velocity and temperature fields of an unsteady Hartmann flow, *Canadian Journal of Physics,* Vol. 76, No. 9, pp. 739, 1998.

[24] K.-L. Hsiao, To promote radiation electrical MHD activation energy thermal extrusion manufacturing system efficiency by using Carreau-Nanofluid with parameters control method, *Energy,* Vol. 130, pp. 486-499, 2017.

[25] K.-L. Hsiao, Combined electrical MHD heat transfer thermal extrusion system using Maxwell fluid with radiative and viscous dissipation effects, *Applied Thermal Engineering,* Vol. 112, pp. 1281-1288, 2017.

[26] M. Chaudhary, J. Merkin, Free-convection stagnation-point boundary layers driven by catalytic surface reactions: I the steady states, *Journal of Engineering Mathematics,* Vol. 28, No. 2, pp. 145-171, 1994.

[27] J. Ramana Reddy, V. Sugunamma, N. Sandeep, Effect of frictional heating on radiative ferrofluid flow over a slendering stretching sheet with aligned magnetic field, *The European physical journal plus,* Vol. 132, No. 1, pp. 7, 2017.

[28] J. V. R. Reddy, V. Sugunamma, N. Sandeep, Effect of nonlinear thermal radiation on MHD flow between rotating plates with homogeneous-heterogeneous reactions, *International Journal of Engineering Research in Africa,* Vol. 20, pp. 130-143, 2016.

[29] J. Raza, A. M. Rohni, Z. Omar, Numerical investigation of copper-water (Cu-water) nanofluid with different shapes of nanoparticles in a channel with stretching wall: slip effects, *Mathematical and Computational Applications,* Vol. 21, No. 4, pp. 43, 2016.

[30] J. Merkin, A model for isothermal homogeneous-heterogeneous reactions in boundary-layer flow, *Mathematical and Computer Modelling,* Vol. 24, No. 8, pp. 125-136, 1996.